Transmission electron microscopy study of extended defect evolution and amorphization in silicon carbide under silicon ion irradiation

Jean-Marc Costantini, Joel Ribis

TRANSMISSION ELECTRON MICROSCOPY STUDY OF EXTENDED DEFECT EVOLUTION AND AMORPHIZATION IN SILICON CARBIDE UNDER SILICON ION IRRADIATION

Jean-Marc COSTANTINI[1], and Joël RIBIS,

Université Paris-Saclay, CEA, Service de Recherches Métallurgiques Appliquées, 91191, Gif-sur-Yvette, France

ABSTRACT

The damage induced in 3C-SiC epilayers on a silicon wafer by 2.3-MeV Si ion irradiation for fluences of 10^{14}, 10^{15}, and 10^{16} cm^{-2}, was studied by conventional and high-resolution transmission electron microscopy (TEM/HRTEM). The evolution of extended defects and lattice disorder is followed in both the 3C-SiC film and Si substrate as a function of ion fluence, with reference to previous FTIR spectroscopy data.

The likelihood of athermal unfaulting of native stacking faults by point defect migration to the native stacking faults is discussed in relation to damage recovery. Threshold energy densities and irradiation doses for dislocation loop formation and amorphous phase transformation are deduced from the damage depth profile by nuclear collisions. The role of electronic excitations on the damage recovery at high fluence is also addressed for both SiC and Si.

Keywords: Silicon carbide; silicon; ion irradiation; amorphization; damage recovery; TEM; HRTEM

[1] Corresponding author's email : jean-marc.costantini@cea.fr

I. INTRODUCTION

Silicon carbide is an important material for use in harsh environments such as for nuclear energy applications [*1, 2*] as well as for microelectronics at high temperature [*3*]. The polytypism arising from different stacking of the Si and C atomic layers is known to be a key factor for understanding the physical properties of SiC [*4*]. The cubic 3C-SiC, with the so-called β-SiC crystal structure, is recognized as the most stable polytype, as confirmed by recent free energy calculations [*5, 6*]. Moreover, the knowledge of extended defect formation such as stacking faults (SFs) and twins in the various polytypes is an important issue for use in electronic devices, since these defects can significantly modify the band structure and deteriorate their electronic properties [*7, 8*]. Moreover, 4H/6H SiC-based devices were found to degrade under operation due to partial Shockley SF formation and expansion [*9, 10*]. As a matter of fact, localized electronic states are generated in the band gap by SFs [*11*]. It was evaluated that the formation energy of SFs in SiC is actually much smaller than in silicon or carbon [*12, 13*]. The SFs in the 6H polytype can generate a disorder in the hexagonal crystal structure of α-SiC which induces an extra Raman-active band at 796 cm^{-1} arising from a phonon mode at the Brillouin zone edges [*13*]. For 3C-SiC, only one kind of SFs is possible in the {111} plane family [*14-16*] with a missing B layer in the ABCABCABC stacking [*7*].

The mechanism of SF formation during crystal growth and the SF formation energy in the various polytypes was the topic of a long-standing debate during the last decade still to date [*6, 16-18*]. There is a strong temperature dependence of the SF formation energy in SiC [*6*]. However, unfaulting in SiC by dislocation reactions is a fairly unknown topic, unlike for silicon [*19*].

For the nuclear applications or ion implantation processes, many studies have shown that amorphization (loss of long-range atomic order) can be achieved in SiC by accumulation of point defects (Frenkel pairs and anti-site defects) and defect-cluster formation above a threshold irradiation dose (or fluence) under energetic electron [*20*] or ion [*21*] beams. Complete amorphization of SiC is achieved in two stages in agreement with Molecular Dynamics (MD) simulations [*22*]: i) a first stage (I), for a damage fraction of $f_D < 0.15$, corresponds to point defect

accumulation (to reach amorphization) and ii) a second one (II) of amorphous domain overlap for f_D > 0.15 [*23, 24*]. No direct amorphization is achieved by a single ion impact in one atomic displacement cascade. The progressive loss of long-range order was seen by the vanishing and broadening of the narrow Raman peaks associated to phonon modes of 4H- and 6H-SiC [*25*]. A progressive band-gap narrowing was measured by UV-visible absorption spectroscopy [*26*]. This was also accompanied by an increase of the backscattering yield in Rutherford backscattering spectroscopy-channeling (RBS/C) experiments on 6H-SiC single crystals, corresponding to disorder build-up in the Si sublattice [*23, 27*]. FTIR spectroscopy data have also shown a progressive decrease and broadening of the TO (at 790 cm^{-1}) and LO (at 970 cm^{-1}) phonon peaks of 3C-SiC epilayers that are consistent with the former results by Raman spectroscopy finding a threshold amorphization fluence corresponding to ~0.3-0.4 displacement per atom (dpa) [*28*].

Previous results have reported the effect of SFs on the enhanced radiation resistance of nanocrystalline SiC [*29*]. The impact of extended defects, such as native SFs, on the behavior of bulk SiC under irradiation and the evolution of SFs are topics that need be investigated. In order to address these issues, transmission electron microscopy (TEM/HRTEM) results are reported on virgin and ion irradiated 3C-SiC epilayers on a Si substrate. Those data are found to be consistent with the previous FTIR spectroscopy data [*28*]. The evolution of native SFs of the pristine 3C polytype and its impact on radiation damage are discussed. The likelihood of athermal unfaulting induced by point defect accumulation and migration to SFs is also addressed.

II. EXPERIMENTAL PROCEDURES

Epitaxial films of 3C-SiC (100) on a Si (100) substrate supplied by the NOVASIC Corp. (Le Bourget du Lac, France) [*30*] were irradiated at the JANNUS-Saclay facility with 2.3-MeV Si ions at room temperature (RT) for fluences of 10^{14}, 10^{15}, and 10^{16} cm^{-2}. The 3C-SiC layers with the cubic zinc blende (ZnS) structure are 1.1-µm thick and the Si wafer is 500-µm thick. The mean projected longitudinal range of the ions is R_p = 1.24 $\pm$ 0.12 µm in SiC according to SRIM2013 calculations [*31*].

Nuclear (S_n) and electronic (S_e) stopping powers of S_n ~63 keV μm^{-1} and S_e ~2.9 MeV μm^{-1}, respectively, are also computed with the SRIM2013 code for the incident ion energy (2.3 MeV). The energy of self-ion irradiation was chosen so as to match the thickness of SiC epilayers. Following recent recommendations [*32*], full cascade simulations are performed for the SiC/Si sample and yield $R_p = 1.32 \pm 0.16$ µm (Fig. 1) by using densities of 3.31 g cm^{-3} for SiC and 3.21 g cm^{-3} for Si. The Si ions are transmitted through the SiC film and stopped in the Si substrate with a damage peak at ~200 nm below the SiC/Si interface (Fig. 1, inset). The major contribution to displacement damage lies in the end-of-range region in the Si substrate.

The total number of displaced atoms and vacancies per incident ion in the SiC/Si sample are of ~4000 and ~3800, respectively, by using the recommended threshold displacement energies of E_d = 35 eV for Si and E_d = 21 eV for C [*33*]. For the SiC film only, the full-cascade simulation gives a total number of displaced atoms and vacancies per incident ion of ~1540 and ~1500, respectively. This yields a total number of displaced atoms per ion path length of (dN_d/dx) ~$1.4x10^3$ μm^{-1} for the SiC film. This value is slightly larger than our previous simulation with the quick damage mode ($1.1x10^3$ μm^{-1}) [*28*]. Similar simulations are also carried out in the Si substrate (E_d = 15 eV) for the Si ion energy of E~160 keV at the SiC/Si interface. One finds a total number of displaced Si atoms and vacancies per incident ion of ~2160 and ~2000, respectively, for $R_p = 218 \pm 67$ nm in Si. This yields a value of (dN_d/dx) ~$1x10^4$ μm^{-1} for the Si substrate. The nuclear-collision damage depth profiles in SiC and Si are shown in Figure 1 (inset).

The TEM and HRTEM observations were performed on a JEOL 2010F electron microscope operating at 200 keV. The FIB lamellae were extracted from the virgin and irradiated samples by focused ion beam (FIB) technique using a standard cross-section preparation with FEI Helios SEM/FIB dual beam microscope.

III. RESULTS

The SiC/Si interface in the virgin sample is found to be rectilinear and of good quality. The cubic structure of the 3C polytype (a = 0.43 nm) with the epitaxial relationship to the cubic diamond structure of Si (a = 0.54 nm) is found from the fast Fourier transform of HRTEM images acquired at the SiC/Si interface (Fig. 2a): it corresponds to a cube-on-cube relationships, i.e. $(100)_{Si}//(100)_{SiC}$ and $[001]_{Si}//[001]_{SiC}$. SFs and twinning joints are observed in SiC with a clear contrast (Figs. 2b and 2c). This is consistent with the X-ray diffraction data showing the presence of twins for (100)-oriented 3C-SiC films on (100) Si [*30*]. The intrinsic or extrinsic nature and orientation of SFs need to be determined. However, the majority of SFs are known to be extrinsic since the formation energy of extrinsic SFs is lower than that of intrinsic ones [*12, 29*]. A SF density of $6x10^{20}$ m^{-3} is estimated in the present virgin SiC film, considering that the FIB lamella is 100-nm thick.

For the ion fluence of 10^{14} cm^{-2}, the radiation damage in the Si substrate up to a thickness of ~200 nm (Fig. 3) is in good agreement with the peak of the nuclear damage depth profile (Fig. 1). The damage consists of small dislocation loops with an average diameter of 5.7 nm. Some loops ranging between 8 nm and 20 nm in size are also seen in the SiC film near the interface, over a thickness of ~400 nm, whereas no damage is found in the rest of the thickness on ~700 nm (Fig. 3). No amorphization of the SiC layer and Si substrate is found for this fluence.

For 10^{15} cm^{-2}, the amorphization of Si is observed up to a thickness of ~400 nm, and the SiC film is also amorphized over the thickness of ~400 nm below the interface (Fig. 4). The amorphized thickness of Si is consistent with the nuclear damage depth profile (Fig. 1, inset). The density of SFs is decreased in the crystalline zone of SiC with respect to 10^{14} cm^{-2}. The SF density is estimated to ~$5.5x10^{20}$ m^{-3} for 10^{14} cm^{-2}, and ~$1.1x10^{20}$ m^{-3} for 10^{15} cm^{-2}.

For 10^{16} cm^{-2}, no amorphization of Si is seen, but rather a damaged zone over the thickness of ~400 nm below the interface (Fig. 5). Figure 6a shows a TEM image of the damaged zone proving that the contrasts observed in Figure 5 are due to the formation of dislocation loops in the Si substrate. Figures 6a and 6b are HRTEM images of a loop showing the $(1\bar{1}1)$ loop habit plane and its

SF. The amorphous zone of SiC is increased up to the total film thickness of ~1100 nm. HRTEM images show that the SiC film is still crystalline for 10^{14} cm^{-2} (Fig. 3), while the HRTEM image for 10^{16} cm^{-2} proves the amorphization of SiC (Fig. 5). No SFs are observed in SiC for 10^{16} cm^{-2}.

IV. DISCUSSION

A good overall agreement of the present TEM/HRTEM observations is found with the previous FTIR measurements as a function of ion fluence [*28*]. It helps analyze the contributions of the amorphous and crystalline SiC phases of different thicknesses on the evolution of the TO and LO phonon peaks after ion irradiation. For 10^{14} cm^{-2}, the SiC film is not amorphized in good agreement with the FTIR spectrum only showing a slight decrease in intensity and increase in bandwidth of the prominent TO phonon peak. An asymmetry factor of the Gaussian profile had to be used to fit these peaks. For 10^{15} cm^{-2}, a decrease of the TO phonon peak width was found, whereas the LO phonon peak was clearly broadened. For 10^{16} cm^{-2}, the large broadening of the merged TO and LO phonon peaks with a standard Gaussian shape is consistent with the full amorphization of the film [*28*]. Note that FTIR measurements are not sensitive to modifications of the Si substrate due to the homonuclear Si-Si bonds [*34*].

The anisotropically-oriented SFs in the virgin sample likely contribute to the asymmetry of the TO peak in the FTIR spectrum, with two components of the dielectric constant as for prolate ellipsoidal inclusions [*35*]. The asymmetrical broadening of the TO and LO phonon peaks in Raman spectra of 3C-SiC was assigned to SFs randomly distributed in the (111) direction [*36*]. A shoulder also appeared at 768 cm^{-1} growing with decreasing average SF distance. Narrowing of TO/LO phonon peaks occurred for temperatures above 1990 K due to SF annealing [*36*]. There is probably a SF density limit to obtain such anisotropy. Actually, the detection limit for the disorder–induced Raman band recorded at 796 cm^{-1} is ~10^3 cm^{-1} [*13*]. The SF density of $6x10^{20}$ m^{-3} in the present virgin SiC film corresponds to $6x10^4$ cm^{-1}, considering a 100-nm thick FIB lamella.

The decrease in the number of SFs in the crystalline zone of the SiC film for the ion fluence of 10^{15} cm^{-2} with respect to 10^{14} cm^{-2} is a possible explanation of the unexpected decrease of the TO phonon peak width in the FTIR spectrum, whereas the LO phonon peak width was found to increase significantly [*29*]. The twinning joints acting as diffusion wells for defects can actually play a role on the elimination of point defects and the unfaulting for this fluence. The effect of SFs on the healing of damage in crystalline SiC can be followed by the decrease of the SF density as a function of fluence, from $6x10^{20}$ m^{-3} for the pristine sample, to $\sim 5.5x10^{20}$ m^{-3} for a fluence of 10^{14} cm^{-2}, and $\sim 1.1x10^{20}$ m^{-3} for 10^{15} cm^{-2}.

The exponential decay of the normalized SF density (Fig. 7) yields a damage cross section of $\sigma = 1.63x10^{-15}$ cm^2 which can be compared to the damage cross section ($\sigma = 1.1x10^{-16}$ cm^2) deduced from the LO phonon peak evolution for these samples [*29*]. The curve of damage fraction calculated from: $f_D = 1 - \exp(-\sigma\phi)$, by using the latter σ value, is plotted with the normalized SF density data (Fig. 7). The curve to reach full amorphization ($f_D = 1$) for $\phi = 10^{16}$ cm^{-2} is also plotted by using a value of $\sigma = 3.5x10^{-16}$ cm^2. The latter curve must be considered as an upper boundary of f_D-values in the fluence range between 10^{14} and 10^{16} cm^{-2}, whereas the FTIR data certainly underestimates the f_D-values due to the merging of the TO and LO phonon peaks as the damage proceeds. Those two curves encompass the range of f_D-values for these samples.

It is seen that the SF density steeply decays in a fluence range corresponding to the stage I of point-defect accumulation for $f_D < 0.15$ (marked by dividing lines in Fig. 7). During this stage, point defects can diffuse out to the SFs thereby causing unfaulting. The role of the various point defects (Si and C Frenkel pairs, Si_C and C_{Si} anti-sites) is an important factor to be considered on the unfaulting by migration to SFs.

Actually, the effect of SFs in reducing the damage in electron-irradiated nanocrystalline SiC with respect to the single crystal was already observed by TEM and supported by MD simulations [*30*]. It was found that the extrinsic SFs lower the energy barriers of Si interstitial migration and anti-

site defect (Si_C) recombination reaction, thereby enhancing point defect annihilation. Moreover, a*b-initio* calculations showed that configurations of Si interstitials are strongly modified near SFs [*37*].

The evolution of the SiC epilayer as a function of ion fluence in the crystalline and amorphous zones may be assessed by a kinetic model to determine the stationary equilibrium regime for a given fluence by feeding in the point defect fluxes to SFs and the film/substrate interface [*38*]. However, such analysis is out of the scope of the present paper only highlighting the main experimental features of radiation damage in 3C-SiC films.

The threshold stopping power and total dpa for the appearance of dislocation loops in SiC and amorphization for fluences of $\phi = 10^{14}$ and $\phi = 10^{15}$ cm^{-2}, respectively, can be determined from the nuclear collision damage depth profile deduced from the SRIM2013 simulations to the depth of 700 nm in the SiC epilayer (Fig. 1). The threshold stopping power value is of S_n ~150 keV μm^{-1} on the latter damage profile to reach this depth, whereas the electronic stropping power is steadily decreasing to the value of S_e ~1300 keV μm^{-1} at this depth. This confirms that damage is definitely created by nuclear collision processes by accumulation of point defects, in agreement with the previous experimental results [*24, 25*] and MD simulations [*23*]. However, since S_e is much larger than S_n over the whole film thickness, this may lead to some partial damage recovery, as found for swift heavy ion irradiation with similar relative S_e and S_n depth dependences [*39*]. A contribution of electronic excitations to the dynamic annealing of damage was also suggested [*21*].

IV.1 Threshold energy densities for amorphization and dislocation loop formation

IV.1.a. Amorphization

According to the homogeneous amorphization mechanism for silicon, amorphization occurs when the lattice energy increases over a critical energy density (E_c) corresponding to a critical defect concentration [*40*]. The critical fluence to reach amorphization (ϕ_c) is related to E_c as: $\phi_c \, \Delta E/t = E_c$, where ΔE is the energy spent in atomic collisions and t is the amorphous thickness [*40, 41*]. To obtain E_c, $\Delta E/t$ can be replaced by the nuclear stopping power (S_n).

For amorphization of silicon a value of ϕ_c ~$2x10^{14}$ cm^{-2} was obtained for 180-keV Ar ion irradiation at 80 K [*40, 41*]. It was found that ϕ_c increases with temperature due to dynamic annealing [*41*]. For instance, ϕ_c ~$3x10^{14}$ cm^{-2} for 180-keV N ion irradiation at 80 K, and ϕ_c ~$1x10^{16}$ cm^{-2} at 300 K, due to vacancy diffusion out of the collisions cascades and point defect annihilation [*40*]. For RT irradiations, the damage also increases with the dose rate [*41*]. For higher temperatures (> 370 K) in silicon, ϕ_c decreases with the beam current [*41*].

By applying such a model to SiC, an energy density of $E_D = S_n \phi$ ~$1.5x10^{24}$ eV cm^{-3} is deduced for $\phi = 10^{15}$ cm^{-2}, at the 700-nm depth in the SiC film, for the ion energy of E ~700 keV and S_n ~150 keV μm^{-1} (Fig. 1), using a mean atom density of $N_a = 9.6x10^{22}$ at cm^{-3}. This gives a threshold energy density of E_D ~15 eV at^{-1} to reach amorphization of SiC, since S_n is increasing below 700 nm. By taking the average value of S_n ~245 keV μm^{-1} in the amorphous zone between depths of 700 and 1100 nm, it yields E_D ~$2.5x10^{24}$ eV cm^{-3} ~26 eV at^{-1}. These estimates must be considered as upper boundaries of E_D in the available fluence range between 10^{14} and 10^{16} cm^{-2}. Actually, RBS/C spectroscopy data have shown that the critical E_D value for amorphization of 6H-SiC is ranging between $1.2x10^{24}$ eV cm^{-3} (~12 eV at^{-1}) and $2.4x10^{24}$ eV cm^{-3} (~25 eV at^{-1}) for various ion species and energies at RT and 77 K, regardless of the ion mass [*42*], in rather good agreement with the present threshold values.

For the Si substrate, a value of S_n ~320 keV μm^{-1} is deduced at the interface for E ~160 keV (Fig. 1). This yields an upper boundary of the threshold value of E_D ~$3.2x10^{24}$ eV cm^{-3} for $\phi = 10^{15}$ cm^{-2}, i. e. ~46 eV at^{-1} for $N_a = 6.9x10^{22}$ at cm^{-3} to reach amorphization of Si. This value is definitely overestimated like for SiC. The real value certainly lies in between 4.6 eV at^{-1} (for $\phi = 10^{14}$ cm^{-2}) and 46 eV at^{-1} (for $\phi = 10^{15}$ cm^{-2}). A critical value of E_D ~10^{24} eV cm^{-3} (~15 eV at^{-1}) was actually found by RBS/C data for 150-keV B ion implantation at 77 K [*43*]. A similar critical E_D value of 10-12 eV at^{-1} was found for RT Ar ion implantation at energies ranging between 10 and 40 keV [*44*]. In principle, self-ion implantation should instead enhance growth of the amorphous layer in the end-of-range region due excess added Si atoms [*45*]. However, damage recovery by electronic excitation might contribute to such a deviation, in agreement with the decrease of the amorphous zone in the Si substrate for

10^{16} cm^{-2}, as compared to 10^{15} cm^{-2}. Actually, the electronic stopping power of the 160-keV Si ions (S_e ~570 keV μm^{-1}) at the SiC/Si interface is larger than the nuclear stopping power (S_n ~320 keV μm^{-1}) in Si (Fig. 1).

IV.1.b. Dislocation loop formation

This gives further confidence to consider the dislocation loop formation in the SiC film. In that case, the value of E_D ~$1.5x10^{23}$ eV cm^{-3}, i.e. 1.5 eV at^{-1} for $\phi = 10^{14}$ cm^{-2}, is also an upper boundary of the threshold value, since we do not have results for fluences lower than 10^{14} cm^{-2}. For silicon, the formation energy of faulted or perfect dislocation loops was found to decrease from ~0.22 eV at^{-1} to ~0.1 eV at^{-1} as a function of loop area [*46*]. Dislocation loops induced by ion implantation in 4H-SiC were found to be produced by condensation of excess Si interstitials [*47, 48*]. The smaller loops (< 5 nm in radius) are very stable up to high temperature (< 2000°C) [*49*]. By contrast, loops produced in the end-of-range region of Si ion implanted silicon were annealed at lower temperature (≤ 1000°C) [*50*]. Therefore, we surmise that the dislocation loop formation energy should be larger for SiC, even though no clear data are available in the literature to our knowledge.

Despite the lack of data on the dislocation loop formation process, it may be assigned to the dumbbell Si interstitial migration with an activation energy ranging between 1.25 eV and 1.6 eV according to experimental data [*51, 52*], and of 1.53 ± 0.02 eV from MD simulations in 3C-SiC [*53*]. Other *ab-initio* computations give values of 1.25 eV [*54*] and 1.4 eV [*55*] for the Si split interstitial migration in 3C-SiC. This value is larger than that of single Si interstitials (0.78 eV) in 3C-SiC [*56*]. The experimental value of activation energy for C interstitial migration is clearly lower (0.89 eV) [*57*] in agreement with the MD simulations (0.74 ± 0.05 eV) [*53*]. Activation energies for vacancy migration are naturally much larger (2.35 eV and 4.10 eV for Si and C, respectively) [*53*].

The ion distribution computed by the SRIM2013 code shows that Si atoms are mainly implanted at a depth between 700 nm and 1.1 µm in the SiC film (Fig. 1). These results are thus consistent with the formation of small dislocation loops resulting from excess Si interstitial migration

and coalescence [*47, 48*] induced above this energy barrier under in-beam conditions at RT, without any thermally-activated diffusion and growth processes.

IV.2 Threshold irradiation doses for amorphization and dislocation loop formation

SRIM2013 simulations give $(dN_d/dx) \sim 1.4x10^3$ μm^{-1} and an upper boundary for the number of dpa = $(dN_d/dx)\ \phi/N_a \sim 0.13$ at $\phi = 10^{15}$ cm^{-2}, for the amorphization below the SiC/Si interface, and dpa ~ 1.3 at $\phi = 10^{16}$ cm^{-2}, for full amorphization of the SiC layer. The present threshold dose for amorphization is thus ranging between ~0.13 and ~1.3 dpa which is consistent with the value determined by RBS/C measurements, i.e. ~0.4-0.5 dpa for SiC amorphization at RT [*23, 27*].

For the Si substrate, the Si ion energy at the interface is of E ~160 keV (Fig. 1, inset) and an upper boundary of the threshold dose for amorphization is ~1 dpa at $\phi = 10^{15}$ cm^{-2} for (dN_d/dx) $\sim 1x10^4$ μm^{-1}. This is consistent with the Raman spectroscopy data for 100-keV Si ion implantation showing almost full amorphization for a fluence of $8.5x10^{14}$ cm^{-2} [*58*] and an irradiation dose of ~1 dpa due to accumulation of point defects (divacancies) [*59*].

The threshold dose for loop formation in SiC is ~0.013 dpa for $\phi = 10^{14}$ cm^{-2}. Actually, MD simulations of displacement damage in SiC by Si ions from 10-keV to 50-keV energies showed that overlap of few atomic collision cascades (5) produces single self-interstitials atoms up to 0.0125 dpa [*60*]. Nanoscale defect clusters are formed by further cascade overlap (~30) above 0.05 dpa, in agreement with experimental HRTEM images [*60*]. Coarsening and accumulation of these clusters were found to lead to amorphization for larger doses.

In summary, when increasing the Si ion fluence, the excess Si interstitials produced by nuclear collisions in the implanted region of the film below the SiC/Si interface (Fig. 1) condense into dislocation loops above 0.01 dpa. For a higher dose, displacement cascade overlaps induce defect cluster accumulation above 0.1 dpa and full amorphization of the SiC film for 1.3 dpa. The SF density decrease with fluence is assigned to some damage healing during the stage I of point-defect buildup. Amorphization of the Si substrate is found in the end-of-range of implanted Si atoms for ~1 dpa.

Values of all threshold energy densities and irradiation doses are reported in Table I. It is known that those NRT-dpa values may be overestimated by the SRIM code, as highlighted in a recent paper suggesting the use of the arc-dpa model including recombination processes [*61*]. Nevertheless, the computed nuclear damage depth profile (Fig. 1) is in very good agreement with the present TEM images (Figs. 3-5).

The decrease of the amorphous zone in the Si substrate for 10^{16} cm^{-2} is a challenging issue. Damage recovery in Si below the interface where $S_e > S_n$ (Fig. 1) is also observed for 10^{15} cm^{-2}, thereby showing that this is a continuous recovery process. Electronic excitations may play a role in the healing of point defects and extended defects. Such an athermal annealing process by electronic excitation is definitely more pronounced in the case of SiC [*21*], for which clear evidence of damage recovery was already found for a much higher S_e value (~17 MeV μm^{-1}) with 95-MeV Xe ion irradiation, with similar relative S_e and S_n depth dependences [*39*] as in the present study. This may induce an increase of the full amorphization dose by nuclear collisions in the SiC film. The low activation energies (< 1 eV) for recombination of close Si Frenkel pairs [*62*] might account for such a damage recovery process, in agreement with the thermal recovery stage of SiC below RT.

However, it is to be noted that S_e values may also be overestimated for slow light ion irradiation of targets containing light elements, such as SiC and Si [*32*]. The CASP 5.0 code [*63*] actually yields a total stopping power of ~4.3×10^{-13} eV cm^2 per SiC molecule for the incident 82-keV u^{-1} Si ion energy using ionization of the 1s, 2s 2p, 3s, and 3p shells, which gives S_e ~2.1 MeV μm^{-1} (for a molar mass of 40 g and mass density of 3.31 g cm^{-3}) instead of 2.9 MeV μm^{-1} as computed by SRIM2013. The DPASS code [*64*] based on the dielectric function theory gives ~6.2×10^{-14} eV cm^2 for Si and ~3.0×10^{-14} eV cm^2 for C, i.e. $S_e \sim 9.2 \times 10^{-14}$ eV cm^2 ~0.45 MeV μm^{-1} by using the Bragg's additivity rule. This highlights the discrepancies between the various codes based on different physical assumptions on the ion slowing down in matter.

V. CONCLUSIONS

TEM and HRTEM are used to follow the radiation damage in 3C-SiC epilayers in thickness of 1.1 µm on a 500-µm thick Si wafer after 2.3-MeV Si ion irradiation for fluences ranging from 10^{14} cm^{-2} to 10^{16} cm^{-2}. The Si ions were transmitted through the film and implanted in the substrate. The overall evolution of the SiC film under irradiation is consistent with the previous FTIR spectroscopy data on those samples showing progressive amorphization of the epilayer.

Small dislocation loops appear in the SiC film over a thickness of ~400 nm below the SiC/Si interface for 10^{14} cm^{-2}. The threshold energy density (~1.5 eV at^{-1}) deposited by nuclear collisions for loop formation corresponds to the energy barrier of Si dumb-bell interstitial migration. The native SF density decrease in SiC with fluence is assigned to in-beam point defect migration to SFs leading to unfaulting and damage recovery in the stage I of point-defect accumulation.

Amorphization is reached in both SiC and Si near the end-of-range region for 10^{15} cm^{-2}, corresponding to ~0.13 dpa and ~1 dpa, respectively The threshold energy density for SiC amorphization (~15 eV at^{-1}) is consistent with previous determinations by RBS/C spectroscopy. The large threshold energy density for amorphization of Si for 10^{15} cm^{-2} and the damage healing in the Si substrate for 10^{16} cm^{-2} with respect to 10^{15} cm^{-2} may be assigned to electronic excitation effects. Such processes may also induce an increase of the irradiation dose (1.3 dpa) to reach full amorphization of the SiC film.

ACKNOWLEGMENTS: The authors are indebted to the JANNUS-Saclay staff for the Si ion irradiation. This work received assistance from the “Agence Nationale de la Recherche” program GENESIS referenced as ANR-11-EQPX-0020 for the FIB equipment.

REFERENCES

[*1*] R. J. Price, Nuclear Technology, 35 (1977) 320.

[*2*] M. K. Meyer, R. Fielding, and J. Gan, J. Nucl. Mater., 371 (2007) 281.

[*3*] N. G. Wright, A. B. Horsfall, and K. Vassilevski, Materials Today, 11 (2008) 16.

[*4*] M. Hundhausen, R. Püsche, J. Röhrl, and L. Ley, Phys. Stat. Sol. (b), 245 (2008) 1356

[*5*] S. Kawanishi, and T. Mizoguchi, J. Appl. Phys., 119 (2016) 175101.

[*6*] E. Scalise, A. Marzegalli, F. Montalenti, and L. Miglio, Phys. Rev. Appl., 12 (2019) 021002.

[*7*] M. S. Miao, S. Limpijumnong, and W. R. L. Lambrecht, Appl. Phys. Lett., 79 (2001) 4360.

[*8*] M. Skowronski, and S. Ha, J. Appl. Phys., 99 (2006) 011101.

[*9*] A. T. Blumenau, R. Jones, , S. Öberg, and P. R. Briddon, and T. Frauenheim, Physica B 340-342 (2003) 160.

[*10*] A. Tanaka et al., J. Appl. Phys., 119 (2016) 095711.

[*11*] H. P. Iwata, U. Lindefelt, S. Öberg, and P. R. Briddon, Phys. Rev. B, 65 (2001) 033203.

[*12*] P. Käckell, J. Furhmüller, and F. Bechstedt, Phys. Rev. B, 58 (1998) 1326.

[*13*] *S.* Nakashima, Y. Nakatake, H. Harima, M. Katsuno, and N. Ohtani, Appl. Phys. Lett., 77 (2000) 3612.

[*14*] W-S. Seo, K. Koumoto, and S. Aria, J. Am. Ceram. Soc., 83 (2000) 2584.

[*15*] H. P. Iwata, U. Lindefelt, S. Öberg, and P. R. Briddon, Physica B, 340-342 (2003) 165.

[*16*] U. Lindefelt, H. P. Iwata, S. Öberg, and P. R. Briddon, Phys. Rev. B, 67 (2003) 155204.

[*17*] M. Y. Khan, Crystal Res. Technol., 30 (1995) 1127.

[*18*] R. E. Stahlbush, K. X. Liu, and M. E. Twigg, IEEE 06CH37728, 44th Annual Reliability Physics Symp., San Jose, 2006, p. 90.

[*19*] T. Y. Tan, Appl. Phys. Lett., 34 (1979) 714.

[*20*] M. Ishimaru, I.-T. Bae, Y. Hirotsu, S. Matsumura, and K. E. Sickafus, Phys. Rev. Lett., 89 (2002) 055502.

[*21*] W. J. Weber, Y. Zhang, and L. Wang, Nucl. Instr. Meth. B, 277 (2012) 1.

[*22*] F. Gao, and W. J. Weber, Phys. Rev. B, 66 (2002) 024106.

[*23*] X. Kerbiriou, J. M. Costantini, M. Sauzay, S. Sorieul, L. Thomé, J. Jagielski, and J. J. Grob, J. Appl. Phys., 105 (2009) 073513.

[*24*] J. M. Costantini, X. Kerbiriou, M. Sauzay, and L. Thomé, J. Phys. D: Appl. Phys., 45 (2012) 465301.

[*25*] S. Sorieul, J. M. Costantini, L. Gosmain, G. Calas, J. J. Grob, and L. Thomé, J. Phys.: Condens. Matter, 18 (2006) 5235.

[*26*] S. Sorieul, J-M Costantini, L. Gosmain, G. Calas, J-J Grob, and L. Thomé, J. Phys.: Condens. Matter, 18 (2006) 8493.

[*27*] W. Jiang, Y. Zhang, and W. J. Weber, Phys. Rev. B, 70 (2004) 165208.

[*28*] J. M. Costantini, S. Miro, and O. Pluchery, J. Phys. D: Appl. Phys., 50 (2017) 095301.

[*29*] L. Jamison, M-J. Zheng, S. Shannon, T. Allen, D. Morgan, I. Szlufarska, J. Nuclear Mater., 445 (2014) 181.

[*30*] M. Portail, M. Zielinski, T. Chassagne, and M. Nemoz, J. Appl. Phys., 105 (2009) 083505.

[*31*] J. P. Biersack, and L. G. Haggmark, Nucl. Instr. and Meth., 174 (1980) 257. (www.srim.org)

[*32*] W. J. Weber, and Y. Zhang, Current Opinion in Solid State and Mater. Sci., 23 (2019) 100757.

[*33*] R. Devanathan, and W. J. Weber, J. Nucl. Mater., 278 (2000) 258.

[*34*] O. Pluchery, and J. M. Costantini, J. Phys. D: Appl. Phys., 45 (2012) 495101.

[*35*] H. Mutschke, A. C. Andersen, D. Clément, Th. Henning, and G. Peiter, Astron. and Astrophys., 345 (1999) 187.

[*36*] S. Rhomfeld, M. Hundghausen, and L. Ley, Phys. Rev. B, 58 (1998) 9558.

[*37*] J. Xi, B. Liu, Y. Zhang, and W. J. Weber, Comput. Materials Sci., 123 (2016) 131.

[*38*] T. R. Allen, and G. S. Was, "*Radiation-Induced Diffusion and Radiation-induced Segregation*", in Radiation Effects in Solids, Eds. By K. E. Sickafus, E. A. Kotomin, and B. P. Uberuaga, NATO Science Series, vol. 235 (Springer, Dordrecht, 2004).

[*39*] A. Audren, I. Monnet, D. Gosset, Y. Leconte, X. Portier, L. Thomé, F. Garrido, A. Benyagoub, M. Levalois, N. Herlin-Boime, C. Reynaud, Nucl. Instr. and Meth. B, 267 (2009) 976.

[*40*] L. Pelaz, L. A. Marqués, and J. Barbolla, J. Appl. Phys., 96 (2004) 5947.

[*41*] J. R. Dennis,and E. B. Hale, Appl. Phys. Lett., 29 (1976) 523.

[*42*] M. G. Grimaldi, L. Calcagno, P. Musumeci, N. Frangis, and J. Van Landuyt, J. Appl. Phys., 81 (1997) 7181.

[*43*] L. A. Christel, J. F. Gibbons, and T. W. Sigmon, J. Appl. Phys., 52 (1981) 7143.

[*44*] A Claverie, C. Vieu, J. Faure, and J. Beauviliain, J. Appl. Phys., 64 (1988) 4415.

[*45*] O. W. Holland, and C. W. White, Nucl. Instr. Meth.B, 186 (2002) 186.

[*46*] F. Christiano, J. Grisolia, B. Colombeau, M. Omri, B. de Mauduit, A. Claverie, L. F. Giles, and N. E. B. Cowen, J. Appl. Phys., 87 (2000) 8420.

[*47*] P. O. Å. Persson, L. Hultman, M. S. Janson, A. Hallén, R. Yakimova, D. Panknin, and W. Skorupa, J. Appl. Phys., 92 (2002) 2501.

[*48*] C. H. Zhang, Y. M. Sun, Y. Song, T. Shibayama, Y. F. Jin, and L. H. Zhou, Nucl. Instr. Meth.B, 256 (2007) 243.

[*49*] A. Hallén, M. S. Janson, A. Yu. Kuznetsov , D. Åberg, M. K. Linnarson, B. G. Svensson, P. O. Persson, F. H. C. Carlsson, L. Storata, J. P. Bergman, S. G. Sridhara, and Y. Zhang, Nucl. Instr. Meth.B, 186 (2002) 186.

[*50*] G. Z. Pan, K. N. Tu, and A. Prussin, J. Appl. Phys., 81 (1997) 78.

[*51*] W. Primak, L. H. Fuchs, and P. P. Day, Phys. Rev., 103 (1956) 1184.

[*52*] W. J. Weber, W. Jiang, and S. Thevuthasan, Nucl. Instr. Meth. B, 175-177 (2001) 26.

[*53*] F. Gao,W. J. Weber, M. Posselt, and V. Belko, Phys. Rev. B, 69 (2004) 245205.

[*54*] T. Liao, and G. Roma, Nucl. Instr. Meth.B, 327 (2014) 52.[*55*] M. Bockstedte,A. Mattausch, and O. Pankratov, Phys. Rev. B, 68 (2003) 205201.

[*56*] T. Liao, G. Roma, and J. Y. Wang, Philos. Mag., 89 (2009) 2271.

[*57*] Y. Zhang, W. J. Weber, W. Jiang, A. Hallén, and G. Possnert, J. Appl. Phys., 91 (2002) 6388.

[*58*] T. Motooka, and O. W. Holland, Appl. Phys. Lett., 58 (1991) 2360.

[*59*] T. Motooka, and O. W. Holland, Appl. Phys. Lett., 61 (1992) 3005.

[*60*] W. J. Weber, F. Gao, R. Devanathan, W. Jiang, C. M. Zhang, Nucl. Instr. Meth. B, 216 (2004) 25.

[*61*] K. Nordlund, S. J. Zinkle, A. E. Sand, F. Granberg, R. S. Averback, R. Stoller, T. Suzudo, L. Malerba, F. Banhart, W. J. Weber, F. Willaime, S. L. Dudarev, and D. Simeone, Nature Commun., 9 (2018) 1084.

[*62*] F. Gao, and W. J. Weber, J. Appl. Phys., 94 (2003) 4248.

[*63*] G. Schiwietz, and P. L. Grande, Phys. Rev. A 84 (2011) 052703. (https://www.helmholtz-berlin.de/people/gregor-schiwietz/casp_en.html)

[*64*] A. Schinner, and P. Sigmund, Nucl. Instr. Meth.B, 460 (2019) 19. (WWW.sdu.dk/DPASS)

Table I: Values of the threshold energy densities (E_D) and irradiation doses for dislocation loop formation and amorphization in the SiC film and Si substrate, deduced from SRIM2013 full cascade simulations [*31*].

Fluence (cm^{-2})	10^{14}	10^{15}	10^{16}
SiC loop formation E_D ($eV\ cm^{-3}/eV\ at^{-1}$)	$1.5x10^{23}/1.5$		
SiC loop formation dose (dpa)	0.013		
SiC amorphization E_D ($eV\ cm^{-3}/eV\ at^{-1}$)		$1.5x10^{24}/15$	
SiC amorphization dose (dpa)		0.13	1.3
Si amorphization E_D ($eV\ cm^{-3}/eV\ at^{-1}$)		$3.2x10^{24}/46$	
Si amorphization dose (dpa)		1	

Figure 1: Depth profiles of the nuclear (S_n) (solid) and electronic (S_e) (dashed) stopping powers of 2.3-MeV Si ions in SiC and 160-keV Si ions in Si, for the SiC/Si sample irradiated with 2.3-MeV Si ions, and Si ion concentration profile in the SiC film for a fluence of 10^{15} cm^{-2} (dotted, blue) computed with the SRIM2013 code [31]. The inset shows the plot of the Si ion energy (solid) and total target displaced atoms (dotted, green) versus depth.

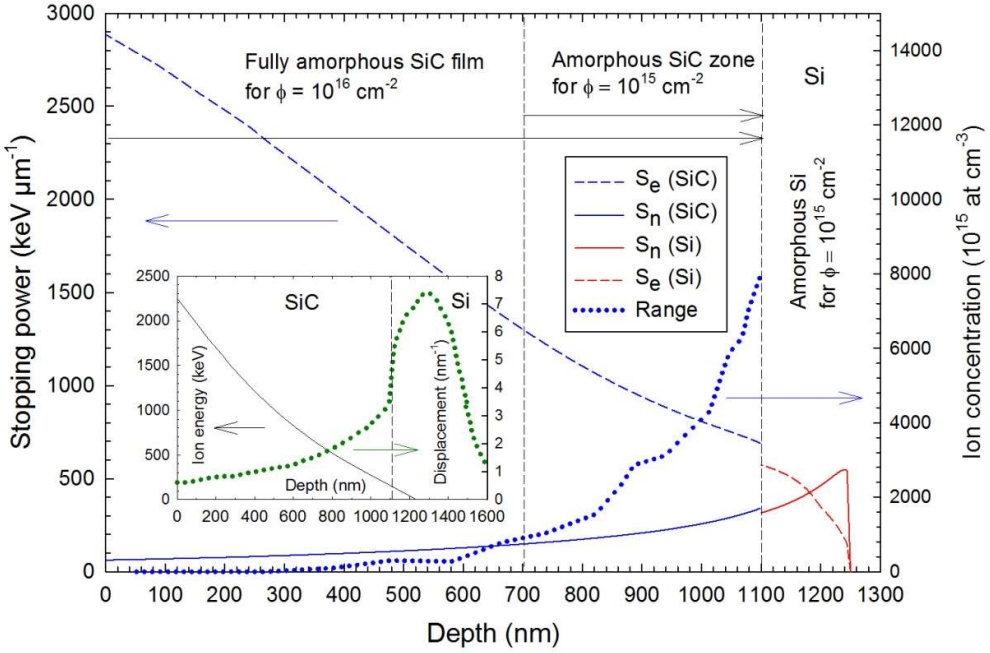

Figure 2: TEM images and electron diffraction pattern of the virgin SiC/Si sample interface (a), and twins in the SiC epilayer (b and c).

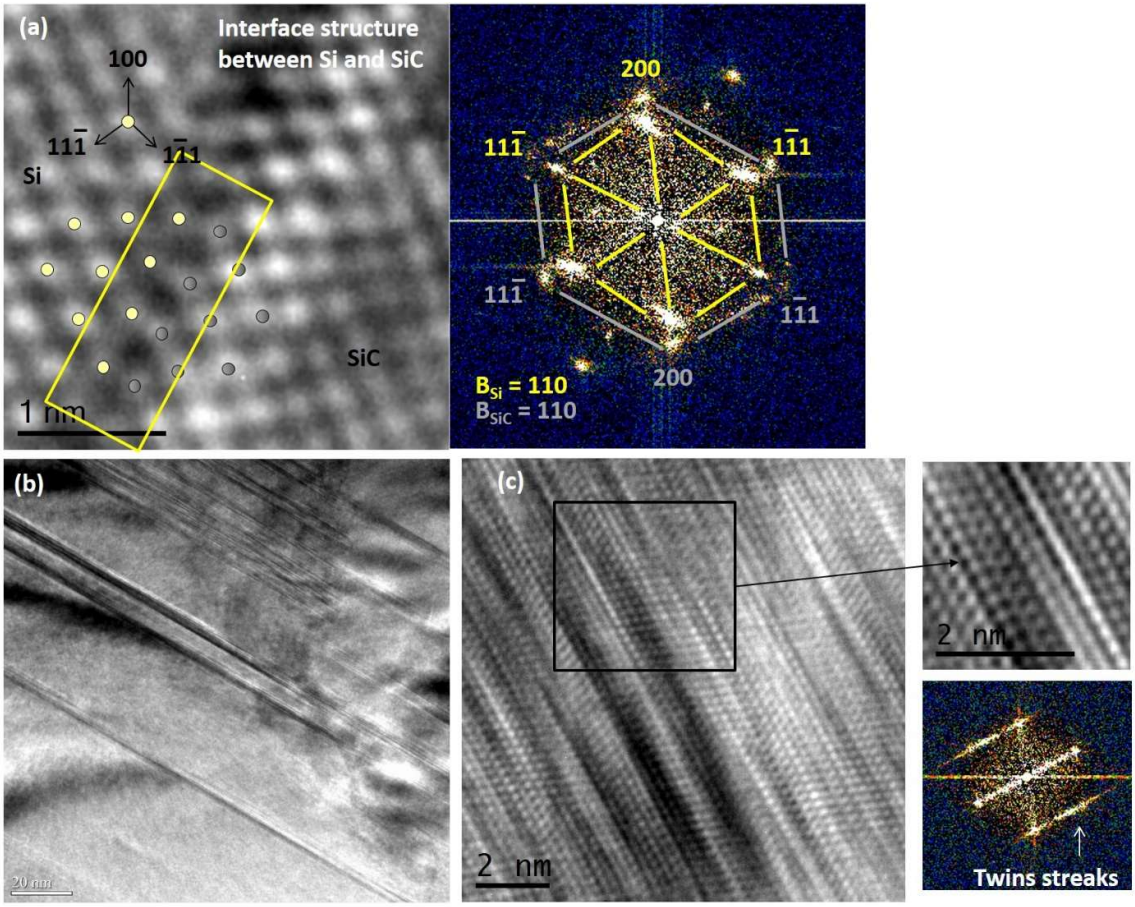

Figure 3: TEM images of the SiC/Si sample irradiated with 2.3-MeV Si ions for a fluence of 10^{14} cm^{-2}.

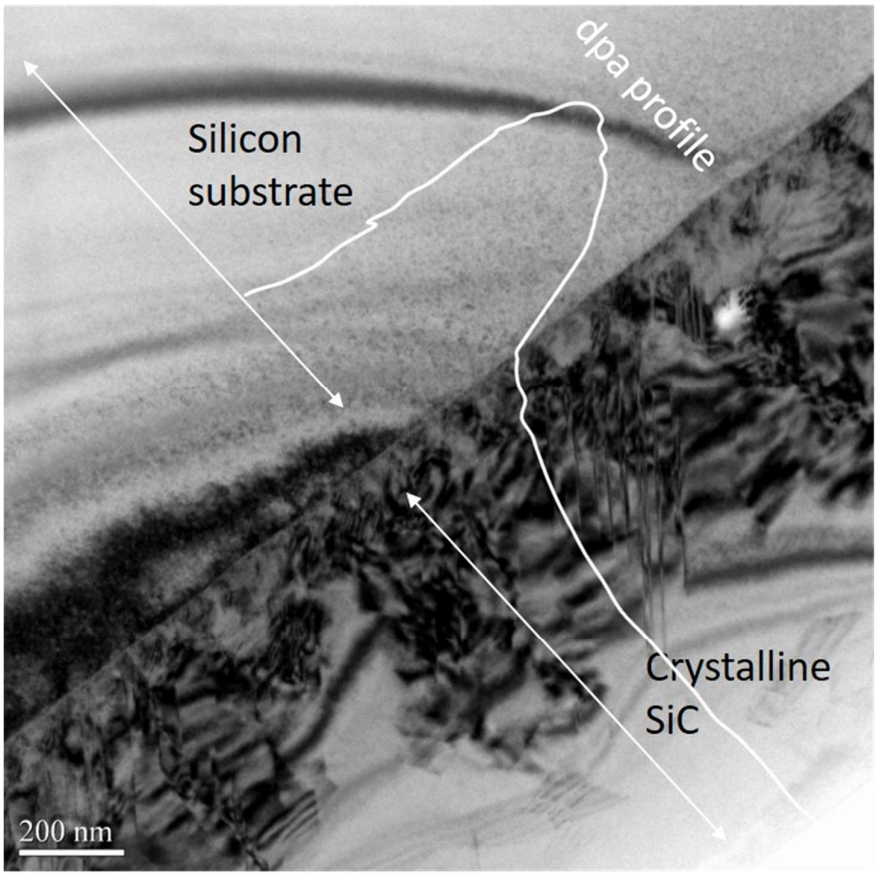

Figure 4: TEM images of the SiC/Si sample irradiated with 2.3-MeV Si ions for a fluence of 10^{15} cm^{-2}.

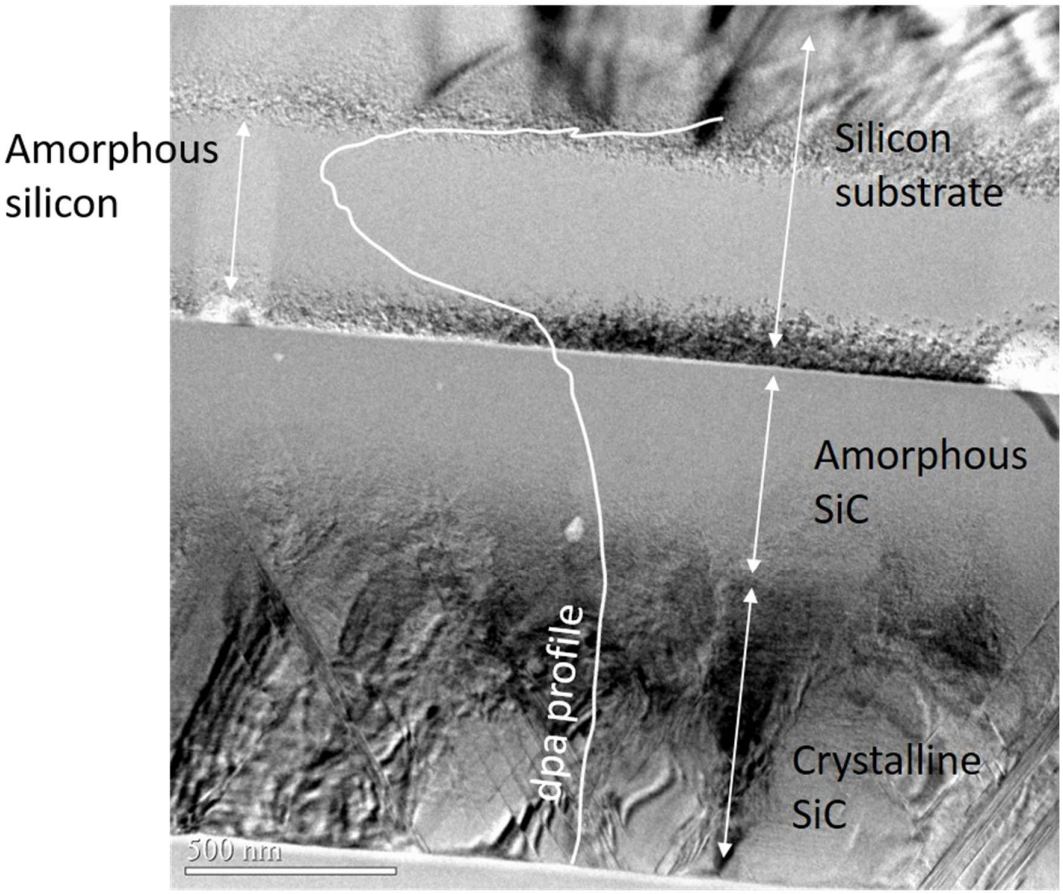

Figure 5: TEM images of the SiC/Si sample irradiated with 2.3-MeV Si ions for a fluence of 10^{16} cm^{-2}.

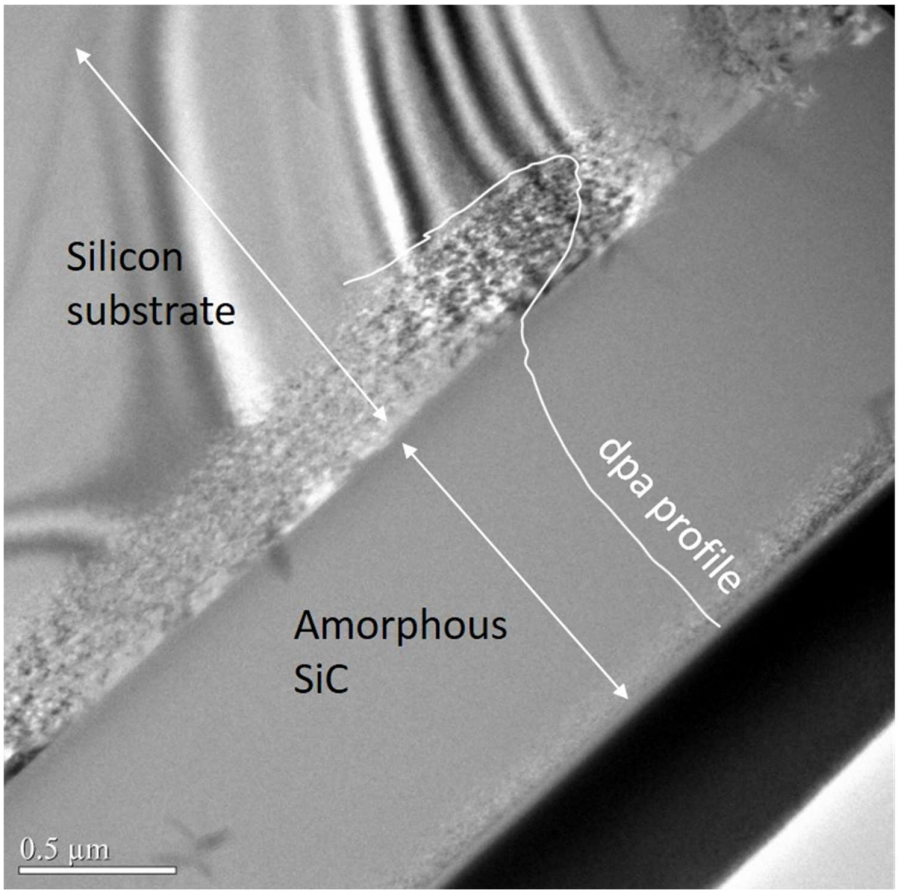

Figure 6: HRTEM images of the Si substrate irradiated for a fluence of 10^{16} cm^{-2}: dislocation loops (a), HRTEM image of the faulted dislocation loop (b), and detailed view of the faulted loop (c).

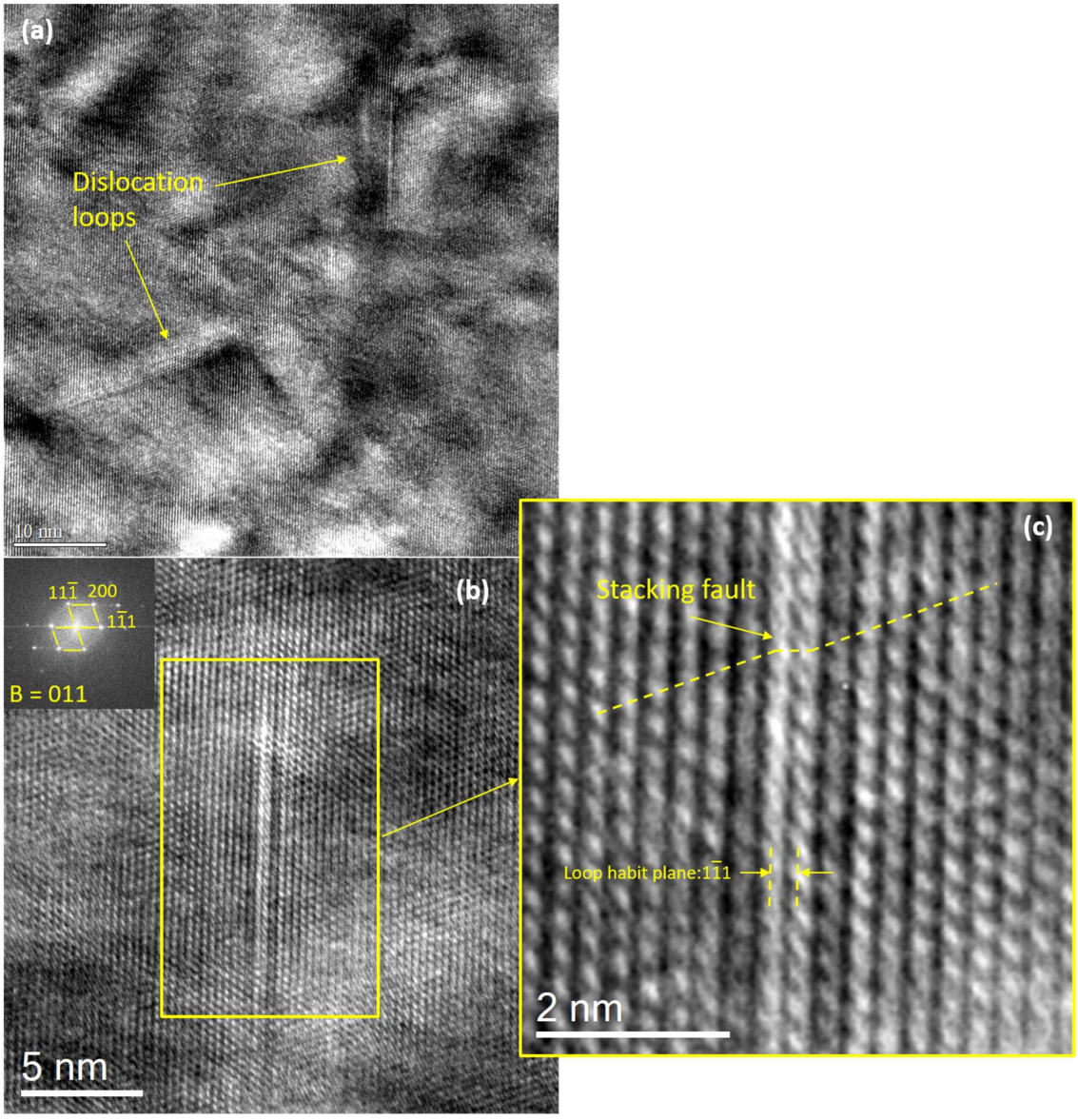

Figure 7: Normalized SF density to the virgin sample value ($6x10^{20}$ m^{-3}) versus fluence (open circles), and calculated curve of damage fraction (f_D) deduced from FTIR data (solid curve) [*30*] and fitted curve to reach f_D ~1 for 10^{16} cm^{-2} (dashed curve). The dotted line is an exponential decay fit. The solid horizontal line marks the transition between stage I and stage II of damage for f_D = 0.15. The upper boundary in fluence of stage I is marked by a vertical solid line.